Stability of Platinum Nanoparticles Supported on SiO_2/Si(111): A High-Pressure X-ray Photoelectron Spectroscopy Study

Soeren Porsgaard,[†] Lindsay R. Merte,[†,‡] Luis K. Ono,[†,‡] Farzad Behafarid,[‡] Jeronimo Matos,[‡] Stig Helveg,[§] Miquel Salmeron,[⊥] Beatriz Roldan Cuenya,[‡,*] and Flemming Besenbacher[†,*]

[†]Interdisciplinary Nanoscience Center (iNANO) and Department of Physics and Astronomy, Aarhus University, DK-8000 Aarhus C, Denmark, [‡]Department of Physics, University of Central Florida, Orlando, Florida 32816, United States, [§]Haldor Topsøe A/S, Nymøllevej 55, DK-2800 Kgs. Lyngby, Denmark, and [⊥]Materials Sciences Division, Lawrence Berkeley National Laboratory, Berkeley, California 94720, United States

ABSTRACT The stability of Pt nanoparticles (NPs) supported on ultrathin SiO_2 films on Si(111) was investigated *in situ* under H_2 and O_2 (0.5 Torr) by high-pressure X-ray photoelectron spectroscopy (HP-XPS) and *ex situ* by atomic force microscopy (AFM). No indication of sintering was observed up to 600 °C in both reducing and oxidizing environments for size-selected Pt NPs synthesized by inverse micelle encapsulation. However, HP-XPS revealed a competing effect of volatile PtO_x desorption from the Pt NPs (~2 and ~4 nm NP sizes) at temperatures above 450 °C in the presence of 0.5 Torr of O_2. Under oxidizing conditions, the entire NPs were oxidized, although with no indication of a PtO_2 phase, with XPS binding energies better matching PtO. The stability of catalytic NPs in hydrogenation and oxidation reactions is of great importance due to the strong structure sensitivity observed in a number of catalytic processes of industrial relevance. An optimum must be found between the maximization of the surface active sites and metal loading (*i.e.*, minimization of the NP size), combined with the maximization of their stability, which, as it will be shown here, is strongly dependent on the reaction environment.

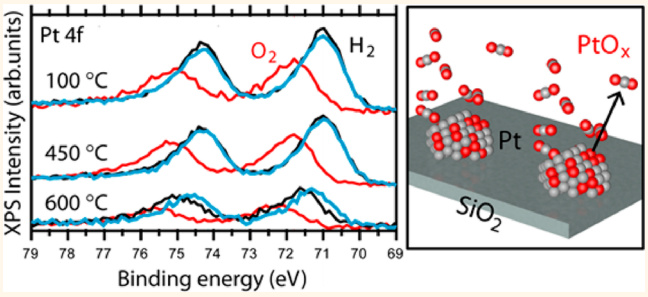

KEYWORDS: platinum nanoparticle · inverse micelle · volatile PtO_x · high-pressure X-ray photoelectron spectroscopy · HP-XPS · atomic force microscopy · AFM

Deactivation of catalytic Pt nanoparticles (NPs) plays an important role in heterogeneous catalysis since Pt NPs are active for a number of industrially relevant reactions such as oxidation of CO and hydrocarbons in automotive catalytic converters, NO_x abatement, volatile organic compound (VOC) combustion, catalytic hydrogenation and reforming, and direct decomposition of alcohols for hydrogen production.[1−4] However, although the smallest Pt NPs may offer desirable properties such as enhanced catalytic activity and selectivity, as well as the economic advantage of minimizing the precious metal loading, short- and long-term stability issues unfortunately limit their applications. The primary routes to deactivation of Pt NPs are through poisoning, coarsening, dissolution in electrochemical environments, and/or volatilization under gas phase reaction conditions.[5−11] Inherently, NPs are metastable and susceptible to coarsening because the high surface free energy can be minimized by the coarsening process.[12,13] This process is limited kinetically by intraparticle or interparticle diffusion of atomic species.[12] Hence, increased temperatures tend to facilitate sintering. By intraparticle diffusion of atomic species over the surface of the NP, the whole particle can migrate and cause coalescence, that is, fusion with another NP. Alternatively, Ostwald ripening can proceed through interparticle migration of atomic species. Common to both sintering mechanisms is that the catalyst material is preserved on the support

* Address correspondence to roldan@ucf.edu, fbe@inano.au.dk.

Received for review August 31, 2012 and accepted November 9, 2012.

Published online November 09, 2012
10.1021/nn3040167

surface, but the catalytic activity is reduced due to the reduced number of active sites (*i.e.*, decreased surface-to-volume ratio).

Recently, the thermal stability of Pt NPs supported on SiO_2 has been the subject of several studies.[13,14] For example, Simonsen *et al.* observed sintering of physical vapor deposited Pt NPs on SiO_2 and Al_2O_3 under 7.5 Torr of technical air (21% O_2 and 79% N_2) at 650 °C by in situ transmission electron microscopy (TEM), which was attributed to ripening.[13,15] Other previous studies have also discussed accelerated sintering rates in O_2 atmospheres.[12,16] On other supports, such as Al_2O_3, enhanced sintering stability and/or dispersion of Pt NPs has been reported after O_2 exposure at lower temperatures (~400 °C).[17,18] In addition, NP migration and ripening were not observed up to ~700 °C under ultrahigh vacuum (UHV) conditions for micelle-synthesized Pt NPs supported on SiO_2/Si(111).[14,19]

Here, we report on the stability of Pt NPs synthesized by inverse micelle encapsulation and supported on SiO_2/Si(111) at conditions closer to those relevant in industrial applications. Using high-pressure XPS, we have studied the properties of the Pt NPs in the presence of elevated pressures of H_2 and O_2 (0.5 Torr). From *in situ* XPS and *ex situ* AFM data, monodispersed 2 nm Pt NPs on a flat SiO_2/Si(111) substrate show no indication of sintering up to 600 °C in reducing and oxidizing environments. However, it was observed that the stability of catalytically active Pt NPs is hampered by desorption of Pt, presumably as volatile PtO_x species formed above 450 °C in O_2. For material systems with limited diffusivity such as NPs dispersed in a porous support, this PtO_x desorption may result in coarsening of the NPs caused by readsorption of the volatile material.

RESULTS AND DISCUSSION

As depicted in Figure 1a, ~2 nm Pt NPs supported on SiO_2/Si(111), sample S1, were cleaned by annealing in 0.5 Torr O_2 (see also the Experimental Procedure section) followed by reduction in 0.5 Torr H_2 at 400 °C. Subsequently, the temperature was changed to a given temperature (*T*) and measured first in H_2 followed by O_2. This cycle, beginning with reduction in 0.5 Torr H_2 at 400 °C, was repeated for different temperatures (*T*) from 100 to 600 °C. Figure 1b shows HP-XPS spectra of the Pt 4f core level region. The black and blue curves were recorded in H_2 at 400 °C and at the stated temperatures, respectively, while the spectra depicted in red were recorded in O_2 at the temperatures given. The black spectra show a slight, but clear, increase of the Pt^0 $4f_{7/2}$ BE from 70.9 to 71.4 eV, followed by a decrease in the peak intensities with increasing annealing temperature. The BE values of the Pt $4f_{7/2}$ species above are similar to reported values for metallic Pt.[14,19−23] No noticeable changes are observed in the Pt 4f peak shapes with temperature when the Pt NPs are exposed to reducing conditions,

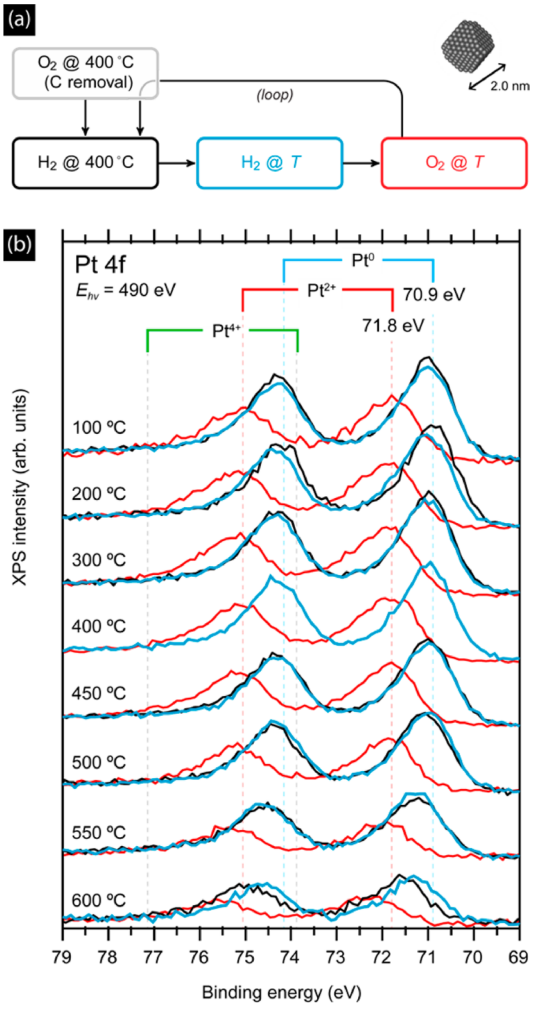

Figure 1. (a) Flow diagram of the HP-XPS measurement steps conducted on sample S1, Pt NPs (~2 nm) supported on SiO_2/Si(111). The sample was initially annealed in O_2 for the removal of residual carbon followed by H_2 for NP reduction. Subsequently, the sample was subjected to heating cycles in 0.5 Torr of H_2 and O_2 at specified temperatures (*T*) increasing in steps from 100 to 600 °C. In each cycle, before annealing at a given temperature in either O_2 or H_2, the sample was measured in 0.5 Torr of H_2 at 400 °C. (b) Series of Pt 4f XPS spectra recorded in 0.5 Torr H_2 at 400 °C (black), 0.5 Torr H_2 at *T* (blue), and 0.5 Torr O_2 at *T* (red). The incident photon energy was 490 eV.

showing a narrow full width half-maximum (fwhm) of 1.1 eV. When the Pt NPs are exposed to O_2, distinct chemical shifts to higher BEs, ranging from 71.7 to 72.0 eV (Pt $4f_{7/2}$), are observed. Since the fwhm values determined from fits of our XPS spectra in O_2 (~1.2 eV) are similar to those in H_2, the presence of a single chemical state is inferred. The presence of significant amounts of PtO_2 can be ruled out based on the reported Pt^{4+} $4f_{7/2}$ BE values from the literature ranging from 73.7 to 74.5 eV.[14,19,24,25] Moreover, if a PtO_2 phase was present, a Pt^{4+} $4f_{5/2}$ peak at ~77.1 eV would be expected. Instead, and in agreement with previous reports,[14,19,21,23,26] the oxide species in our samples is assigned to PtO.

Figure 2a,b shows the changes in the integrated areas and BEs of the Pt 4f XPS peaks, respectively, as

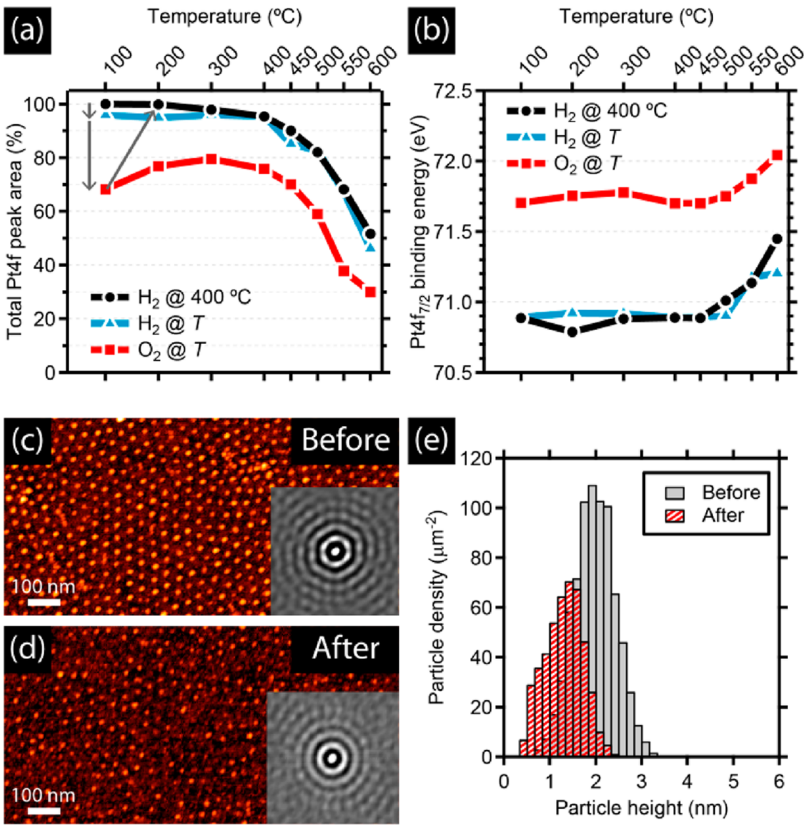

Figure 2. Temperature dependence of the (a) integrated Pt 4f XPS peak areas and (b) Pt $4f_{7/2}$ XPS binding energies of sample S1, Pt NPs (~2 nm) supported on SiO_2/Si(111), in 0.5 Torr H_2 at 400 °C (black circles), 0.5 Torr H_2 at *T* (blue triangles), and 0.5 Torr O_2 at *T* (red squares). The values for the integrated areas are given in percent relative to the first point measured in 0.5 Torr H_2 at 400 °C. Gray arrows indicate the order of the measurements. *Ex situ* AFM images of Pt NPs (c) before and (d) after the high-pressure experiments. (e) NP height histogram extracted from the AFM images. Insets in (c) and (d) show the corresponding autocorrelation images.

a function of the annealing temperature in H_2 (blue triangles) and O_2 (red squares) at specified temperatures (top horizontal axis). Reference data acquired in H_2 at 400 °C after each treatment are also shown (black circles). During each cycle, when the HP-XPS spectra are measured in the presence of O_2 (red squares), the Pt 4f signal intensities appear smaller as compared to those in H_2 at the same temperature. This is attributed to the attenuation of the signal due to the presence of oxygen atoms in the oxide phase and possibly also to reversible shape changes of the Pt NPs in O_2.[27] On the contrary, data measured in H_2 at 400 °C (black circles) after the treatment in O_2 indicate that irreversible changes have taken place. A temperature of ~450 °C is found as the threshold for NP changes, where a strong overall decrease in the Pt 4f peak areas followed by an increase in the BEs is observed. The comparison of the two sequential points (black → blue) in each cycle, Figure 2a, where one corresponds to the measurements in H_2 at 400 °C (black circles) and the second to the subsequent increase in annealing temperature (blue triangles) keeping the same H_2 environment (*e.g.*, 400 °C → 450 °C, 400 °C → 500 °C, 400 °C → 550 °C, and 400 °C → 600 °C), shows no significant differences in the total Pt 4f peak areas. This indicates that the major irreversible changes in the Pt 4f signal are only observed after the Pt NPs are annealed above 450 °C in an O_2 atmosphere.

The origin of the observed intensity attenuation could be assigned to one or more of the following effects: sintering of the Pt NPs, NP shape changes under different gas environments, or loss of Pt from the NPs. In order to elucidate which of these effects contributes the most, *ex situ* AFM measurements of the treated sample S1 ("After") and an identically prepared, untreated sample ("Before") were acquired and analyzed (Figure 2c,d). AFM is suitable not only for measuring the size distribution of the Pt NPs but also for determining their spatial distribution on the support. As a result of the micellar preparation method,[14,28,29] the distribution of Pt NPs exhibits local hexagonal ordering, with uniform interparticle distances determined by the length of the diblock copolymer tails (PS group). The autocorrelation images shown as insets in Figure 2c,d show distinct rings corresponding to the particles' coordination shells, revealing strong local ordering before and after treatment with average NP nearest-neighbor distances of 40 nm in both cases. Thus, sintering of the NPs by particle migration did not occur for our micellar NPs.[4,14,18,19] Figure 2e shows the AFM NP height

histograms of the as-prepared (gray columns) and the treated sample after the HP-XPS measurements (red columns). The NPs in the as-prepared sample had an average height of 2.0 ± 0.5 nm, while those subjected to the high-pressure experiments had an average height of 1.3 ± 0.4 nm. Because NPs smaller than ~0.5 nm are difficult to unambiguously identify in the AFM images due to the rough pearl-like structure of the amorphous SiO_2 support, the precise determination of particle count on the sample after the treatments is difficult. A large number of particles in the range of 0−0.5 nm have not been counted in the latter case, and thus the height distributions obtained from the AFM measurements of the sample after treatment are biased toward a higher average value. Considering the uncounted particles, the true mean height is in the range of 0.8−1.3 nm.

These observations reveal that the decreasing XPS areas obtained with increasing annealing temperature above 450 °C can be primarily assigned to the loss of Pt from the NPs, most likely desorbing as PtO_x during the annealing step in O_2. The other plausible explanations for the XPS signal attenuation, such as sintering or shape change, are ruled out since both would lead to increased or unchanged NP heights in AFM images. Additionally, the positive Pt 4f BE shifts observed as a function of annealing temperature above 450 °C (Figure 2b) corroborate the finding that the Pt NPs become smaller. This conclusion is based on the well-established size-dependent initial and final state effects, which are known to lead to positive BE shifts.[30]

The attenuation in the HP-XPS signal is consistent with the reduction in NP size measured by AFM. If a NP of height h_1 is reduced to a NP of height h_2, and with further assumption that the NP has either spherical or hemispherical shape, the ratio of XPS intensities is given (through application of the Beer−Lambert attenuation law) by

$$\frac{I(h_2)}{I(h_1)} = \frac{1 - \left(1 + \frac{h_2}{\lambda}\right)\exp\left(-\frac{h_2}{\lambda}\right)}{1 - \left(1 + \frac{h_1}{\lambda}\right)\exp\left(-\frac{h_1}{\lambda}\right)} \qquad (1)$$

where λ is the inelastic mean free path (IMFP). From the AFM analysis, the initial NP height was 2.0 ± 0.5 nm (Figure 2e).[31] Thus, if we use 2.0 nm as h_1 in eq 1 and $I(h_2)/I(h_1) = 0.50$, we can then estimate the final NP size numerically. Using the value of 0.733 nm for the IMFP of electrons with a kinetic energy of 420 eV,[32,33] we find a value of 1.0 nm for h_2, which is consistent with the measured AFM height of 0.8−1.3 nm.

In order to verify that the observed loss of Pt is mediated by the elevated pressure of O_2, we have studied the thermal stability of another sample with ~4 nm Pt NPs (S2), exclusively in the presence of O_2 after the initial cleaning in O_2 and reduction in H_2 at 400 °C. The time dependence of the XPS Pt 4f peak area (red circles, left axis) and the temperature (black line, right axis) is shown in Figure 3a. A similar onset temperature of ~450 °C for the drastic Pt 4f XPS attenuation was observed, confirming that the attenuation of the Pt signal detected for S1 at high temperatures was indeed caused by the high pressure of O_2. Figure 3b,c shows AFM images of sample S2 without treatment ("Before") and after the high-pressure experiments ("After"), respectively. On the basis of the autocorrelation images shown in the insets, the interparticle distance is observed to be practically identical before (69 nm) and after (72 nm) HP-XPS measurements. However, the height histograms shown in Figure 3d show a drastic decrease in the NP height from an initial average height of 3.8 ± 1.3 nm to 1.3 ± 0.7 nm. Using eq 1, a 50% decrease in the HP-XPS signal (Figure 3a) leads to an estimated 1.4 nm final NP size, indicating good agreement between the model and AFM results. The IMFP was set to 0.868 nm, corresponding to 550 eV electrons.[32,33]

The loss of Pt from the NPs can be explained in terms of the Pt oxidation kinetics and thermodynamics. The entire NPs were observed to be oxidized in the presence of O_2, but with no indication of PtO_2 formation, in agreement with a report by Wang *et al.*[34] for ~2.0 nm Pt NPs. It should be however noted that there have also been theoretical reports suggesting PtO_2 as the most thermodynamically stable phase for Pt NPs <6 nm under our experimental conditions.[35,36] This finding suggests that the oxidation to PtO_2 is kinetically hindered by O_2 dissociation on the oxidic Pt NPs or by barriers for intraparticle mass transport.[37] This is in agreement with previous reports that PtO, rather than PtO_2, was found to be the predominant species after thermal treatments of supported Pt NPs in O_2,[4,34] and that PtO_2 is observed after atomic oxygen exposure[14,19] where the barrier for dissociative adsorption of O_2 is bypassed. It is plausible that the onset temperatures for PtO_x sublimation[35,38] are lower than the temperature required to overcome the kinetic barrier for PtO_x formation. Consequently, the formation of PtO_x on the NP surface might immediately lead to its desorption. The desorbing species may be PtO_2.

Pt volatilization has been observed in several studies of Pt catalysts under oxidizing conditions similar to those employed here.[12,39−41] For example, Lamber and Romanowski[40] investigated the stability of Pt particles grown on quartz by physical vapor deposition in vacuum and in low pressures of oxygen (2.3×10^{-4} Torr) and observed substantial decreases in crystallite size and Pt mass loss following oxygen treatments at 500 °C, while the vacuum treatments led to NP growth. As discussed by Wynblatt and Gjostein[12] and Harris,[42] vaporization of PtO_2 can contribute to NP coarsening in a similar manner to surface diffusion, *via* the exchange of Pt between particles through an Ostwald ripening process. The fact that only a decrease in NP size during O_2 exposure at high temperature was observed in our

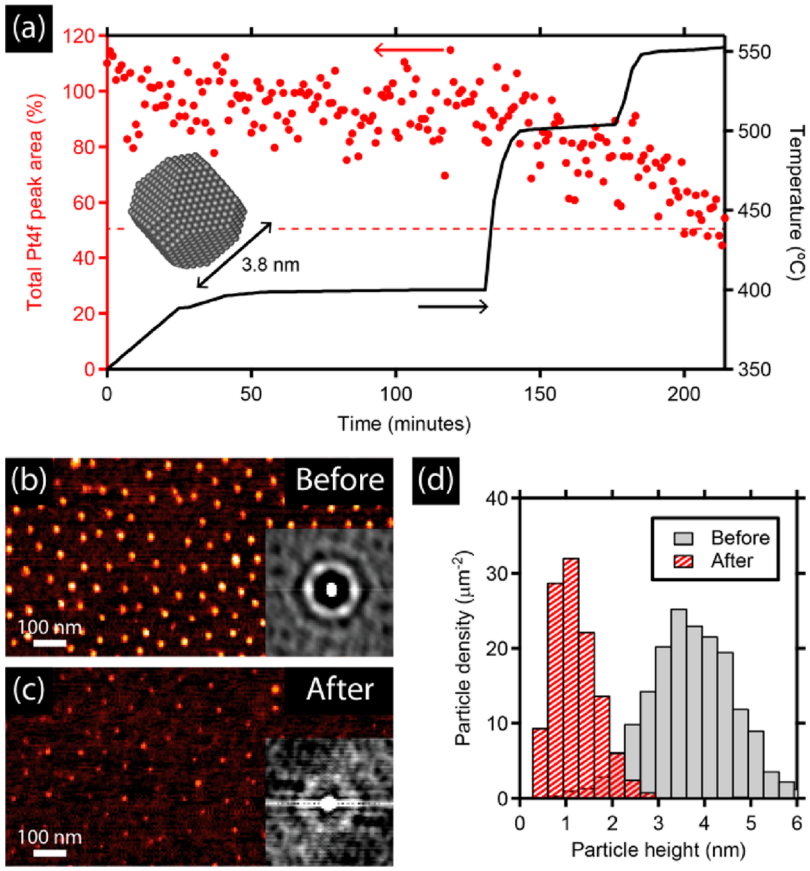

Figure 3. (a) Temperature and time evolution of the integrated Pt 4f XPS peak areas (closed circles) of sample S2, Pt NPs (~4 nm) supported on SiO_2/Si(111), in O_2 atmosphere (0.5 Torr). AFM images of the NPs (b) before and (c) after the high-pressure experiments. (d) Histogram of NP height measurements extracted from the AFM images. Insets in (b) and (c) show the corresponding autocorrelation images. In (a), the XPS spectra were recorded with an incident photon energy of 620 eV.

study and that of Lamber is most likely due to the very low rate of readsorption on our samples due to the planar geometry and the long diffusion length in the gas phase under the conditions of our experiments.

It should be noted that, in the similar studies by Simonsen *et al.* employing *in situ* TEM of Pt NPs on SiO_2 and Al_2O_3, significant coarsening of the NPs was observed in 7.5 Torr technical air (21% O_2 and 79% N_2) at 650 °C without apparent loss of Pt from the surfaces.[13,15] Similar results were obtained by Chu and Ruckenstein,[43] who studied Pt evaporated onto an Al_2O_3 film, though in their case, NP diffusion and coalescence were found to be the primary mode of sintering. In the HP-XPS experiments reported here, the differential pumping of gas into the analyzer causes substantial gas flow near the sample surface, which might help minimize Pt (or PtO_x) redeposition. In the studies by Simonsen and Chu, it is possible that the higher gas pressures and lower gas flows near the surface allowed such redeposition. Potential differences in NP size, shape, and interaction with the support due to the micellar preparation method (exposure to oxygen plasma) may also play a role, as could the initially substantially larger (40−70 nm *vs* ~2−5 nm as in refs 13 and 15) interparticle distances in our samples, potentially allowing diffusing surface PtO_x species to desorb before finding another particle.

The present work highlights the complexity of the fundamental processes underlying catalyst stability and emphasizes the importance of model catalyst studies in gaining a fundamental understanding of the dynamics of NP oxidation and sintering at the nanoscale. Our study suggests that PtO_x volatility plays an important role in catalyst stability under oxidizing conditions.

CONCLUSION

From an interplay of *in situ* HP-XPS and *ex situ* AFM measurements, the thermal stability of micellar Pt NPs supported on SiO_2/Si(111) was investigated under 0.5 Torr of reducing and oxidizing gaseous (H_2 and O_2) environments. No indication of NP sintering (Ostwald ripening or diffusion coalescence) was observed up to 600 °C after exposure to H_2 and O_2, although such an effect could be counteracted by the Pt loss observed in O_2 at temperatures above ~450 °C. When probed under oxidizing conditions, HP-XPS shows a drastic decrease in the Pt 4f signal at temperatures above ~450 °C. It is shown that this irreversible Pt 4f signal

attenuation is caused by the formation of volatile PtO_x species. However, comparison of the AFM autocorrelation images acquired before and after the HP-XPS experiments did not show any clear changes in the spatial distribution of the particles (*i.e.*, NP mobility), indicating the strong adhesion of the particles to the support.

EXPERIMENTAL PROCEDURE

Size-selected Pt NPs were synthesized by the inverse micelle encapsulation technique as described in detail in refs 14, 28, and 29. Briefly, two types of commercially available nonpolar/polar diblock copolymers, poly(styrene)-*block*-poly(2-vinylpyridine) [S1: PS(27700)-*b*-P2VP(4300) and S2: PS(53000)-*b*-P2VP(43800)], were dissolved in toluene in order to form inverse micelles. Subsequently, the micelles were loaded with a $H_2PtCl_6 \cdot 6H_2O$ salt. The size selection was obtained by varying the molecular weight of the polymer core (P2VP) and by changing the metal salt/P2VP ratio. The metal loadings (metal/P2VP ratio) used were 0.2 for S1 and 0.05 for S2. The interparticle distance was determined by the lengths of the nonpolar tails (PS). A monolayer-thick film of polymer-encapsulated Pt NPs was obtained upon dip-coating naturally oxidized amorphous SiO_2/Si(111) substrates into the metal-loaded polymeric solution. The encapsulating polymer was removed in a commercial UHV surface analysis system (SPECS GmbH) *via* an O_2 plasma treatment ($P[O_2] = 3.0 \times 10^{-5}$ Torr for 100 min) at room temperature. Samples with NP sizes of 2.0 ± 0.5 nm (S1) and 3.8 ± 1.3 nm (S2) were obtained by the method described above.

HP-XPS experiments were performed at the beamline 9.3.2 of the Advanced Light Source (ALS) at Lawrence Berkeley National Laboratory.[44,45] The system consists of an analysis chamber with an electron spectrometer mounted on a differentially pumped electrostatic lens system that allows XPS measurements in gas environments up to 1 Torr. The base pressure in this chamber is $\sim 3 \times 10^{-10}$ Torr. O_2 and H_2 gases were dosed individually by backfilling the chamber through a leak valve. Each sample transferred to the HP-XPS analysis chamber was further cleaned *in situ* by annealing in an O_2 atmosphere (0.5 Torr) at 400 °C for 30 min to remove any residual carbon species. After this cleaning procedure, no C 1s signal was observed in XPS. Subsequently, the oxidized Pt NPs were annealed in H_2 (0.5 Torr) at 400 °C, as shown in Figure 1a. After this treatment, the reduction of the NPs was confirmed by XPS. No significant decrease in the Pt 4f intensity was observed after the cleaning and reduction procedures. Samples S1 and S2 received different treatments during the HP-XPS measurements. As depicted in Figure 1a, sample S1 was alternately measured in H_2 (0.5 Torr) and in O_2 (0.5 Torr) for 15 min while keeping the sample at a desired temperature. Prior to each cycle, the sample was annealed at 400 °C in 0.5 Torr of H_2 until XPS showed complete reduction of the PtO_x species to the metallic state. The cycle was repeated by stepwise increasing the temperature for each cycle from 100 to 600 °C, which was the maximum temperature allowed in the experimental setup. Sample S2 was measured only in an O_2 atmosphere (0.5 Torr), monitoring both the temperature and temporal dependence on the Pt 4f signal decay.

The binding energy (BE) scale was calibrated using the Si^0 2p peak at 99.3 eV of the NP substrate [SiO_2(4 nm)/Si(111)]. The BE of Si^0 2p was measured initially using as reference the Au $4f_{7/2}$ (84.0 eV) signal of a small Au foil mounted on the sample holder adjacent to the sample. Quantitative analysis was performed by subtracting a Shirley-type background[46] and fitting each XPS spectrum using two asymmetric Voigt line shapes separated by 3.3 eV corresponding to the spin−orbit splitting of Pt $4f_{7/2}$ and Pt $4f_{5/2}$ peaks.

Characterization of the sample morphology (NP size and interparticle distance) before and after HP-XPS was performed by *ex situ* AFM imaging in tapping mode (Digital Instruments, Multimode). Noncontact silicon AFM tips with an end radius below 10 nm were used. The cantilevers used have resonant frequencies in the range of 200−300 kHz with spring constants between 20 and 30 N/m. A typical scan rate of 1 Hz was used to acquire the AFM images, and the tip−sample interaction was minimized to avoid tip-induced distortions of the NP morphology and NP lateral displacements during scanning. Due to tip convolution effects, the NP height (rather than the diameter) has been used here as representative size parameter.

Beam-induced effects were excluded by changing the sample position at the end of each XPS experiment to confirm that the samples remained homogeneous. The beam spot was 0.5 mm × 1 mm, while the sample size was 9 mm × 9 mm. Thus, beam-induced effects would be easily detected by this procedure. AFM imaging of different areas of the sample showed no indication of inhomogeneity before and after the HP-XPS experiments.

Conflict of Interest: The authors declare no competing financial interest.

Acknowledgment. Authors from iNANO gratefully acknowledge financial support from the Danish Research Agency, the Strategic Research Council, the Villum Kahn Rasmussen Foundation, the Carlsberg Foundation, the Lundbeck Foundation and the European Research Council through an Advanced ERC grant. This work was also supported by the Office of Basic Energy Science of the U.S. Department of Energy under Contract No. DE-FG02-08ER15995 (B.R.C) and Contract No. DE-AC02-05CH11231 (M.S.). The Advanced Light Source is supported by the Director, Office of Science, Office of Basic Energy Sciences, of the U.S. Department of Energy under Contract No. DE-AC02-05CH11231.

REFERENCES AND NOTES

1. Golunski, S. E. Final Analysis: Why Use Platinum in Catalytic Converters? *Platinum Met. Rev.* **2007**, *51*, 162–162.
2. Freund, H.-J. Clusters and Islands on Oxides: From Catalysis *via* Electronics and Magnetism to Optics. *Surf. Sci.* **2002**, *500*, 271–299.
3. Bartholomew, C. H.; Farrauto, R. J. *Fundamentals of Industrial Catalytic Processes*; John Wiley & Sons, Inc.: New York, ISBN: 13 978-0-471-45713-8.
4. Croy, J. R.; Mostafa, S.; Heinrich, H.; Roldan Cuenya, B. Size-Selected Pt Nanoparticles Synthesized *via* Micelle Encapsulation: Effect of Pretreatment and Oxidation State on the Activity for Methanol Decomposition and Oxidation. *Catal. Lett.* **2009**, *131*, 21–32.
5. Forzatti, P.; Lietti, L. Catalyst Deactivation. *Catal. Today* **1999**, *52*, 165–181.
6. Bartholomew, C. H. Mechanisms of Catalyst Deactivation. *Appl. Catal., A* **2001**, *212*, 17–60.
7. Campbell, C. T.; Parker, S. C.; Starr, D. E. The Effect of Size-Dependent Nanoparticle Energetics on Catalyst Sintering. *Science* **2002**, *298*, 811–814.
8. Shao-Horn, Y.; Sheng, W. C.; Chen, S.; Ferreira, P. J.; Holby, E. F.; Morgan, D. Instability of Supported Platinum Nanoparticles in Low-Temperature Fuel Cells. *Top. Catal.* **2007**, *46*, 285–305.
9. Xin, H. L.; Mundy, J. A.; Liu, Z.; Cabezas, R.; Hovden, R.; Kourkoutis, L. F.; Zhang, J.; Subramanian, N. P.; Makharia, R.; Wagner, F. T.; *et al.* Atomic-Resolution Spectroscopic Imaging of Ensembles of Nanocatalyst Particles Across the Life of a Fuel Cell. *Nano Lett.* **2012**, *12*, 490–497.
10. Matsumoto, M.; Miyazaki, T.; Imai, H. Oxygen-Enhanced Dissolution of Platinum in Acidic Electrochemical Environments. *J. Phys. Chem. C* **2011**, *115*, 11163–11169.
11. Merte, L. R.; Behafarid, F.; Miller, D. J.; Friebel, D.; Cho, S.; Mbuga, F.; Sokaras, D.; Alonso-Mori, R.; Weng, T.-C.; Nordlund, D.; *et al.* Electrochemical Oxidation of Size-Selected Pt Nanoparticles Studied Using *In Situ* High-Energy-Resolution X-ray Absorption Spectroscopy. *ACS Catal.* **2012**, *2*, 2371–2376.

12. Wynblatt, P.; Gjostein, N. A. Supported Metal Crystallites. *Prog. Solid State Chem.* **1975**, *9*, 21–58.
13. Simonsen, S. B.; Chorkendorff, I.; Dahl, S.; Skoglundh, M.; Sehested, J.; Helveg, S. Ostwald Ripening in a Pt/SiO_2 Model Catalyst Studied by *In Situ* TEM. *J. Catal.* **2011**, *281*, 147–155.
14. Ono, L. K.; Yuan, B.; Heinrich, H.; Roldan Cuenya, B. Formation and Thermal Stability of Platinum Oxides on Size-Selected Platinum Nanoparticles: Support Effects. *J. Phys. Chem. C* **2010**, *114*, 22119–22133.
15. Simonsen, S. B.; Chorkendorff, I.; Dahl, S.; Skoglundh, M.; Sehested, J.; Helveg, S. Direct Observations of Oxygen-Induced Platinum Nanoparticle Ripening Studied by *In Situ* TEM. *J. Am. Chem. Soc.* **2010**, *132*, 7968–7975.
16. Lööf, P.; Stenbom, B.; Nordén, H.; Kasemo, B. Rapid Sintering in NO of Nanometer-Sized Pt Particles on γ-Al_2O_3 Observed by CO Temperature-Programmed Desorption and Transmission Electron Microscopy. *J. Catal.* **1993**, *144*, 60–76.
17. Fiederow, R. M. J.; Chahar, B. S.; Wanke, S. E. The Sintering of Supported Metal Catalysts II. Comparison of Sintering Rates of Supported Pt, Ir, and Rh Catalysts in Hydrogen and Oxygen. *J. Catal.* **1978**, *51*, 193–202.
18. Matos, J.; Ono, L. K.; Behafarid, F.; Croy, J. R.; Mostafa, S.; DeLaRiva, A. T.; Datye, A. K.; Frenkel, A. I.; Roldan Cuenya, B. *In Situ* Coarsening Study of Inverse Micelle Prepared Pt Nanoparticles Supported on γ-Al_2O_3: Pretreatment and Environmental Effects. *Phys. Chem. Chem. Phys.* **2012**, *14*, 11457–11467.
19. Ono, L. K.; Croy, J. R.; Heinrich, H.; Roldan Cuenya, B. Oxygen Chemisorption, Formation, and Thermal Stability of Pt Oxides on Pt Nanoparticles Supported on SiO_2/Si(001): Size Effects. *J. Phys. Chem. C* **2011**, *115*, 16856–16866.
20. Björneholm, O.; Nilsson, A.; Tillborg, H.; Bennich, P.; Sandell, A.; Hernnäs, B.; Puglia, C.; Mårtensson, N. Overlayer Structure from Adsorbate and Substrate Core Level Binding Energy Shifts: CO, CCH_3 and O on Pt(111). *Surf. Sci.* **1994**, *315*, L983–L989.
21. Wagner, C. D.; Naumkin, A. V.; Kraut-Vass, A.; Allison, J. W.; Powell, C. J.; Rumble, J. R. NIST X-ray Photoelectron Spectroscopy Database, NIST Standard Reference Database 20, version 3.5, **2003**.
22. Puglia, C.; Nilsson, A.; Hernnäs, B.; Karis, O.; Bennich, P.; Mårtensson, N. Physisorbed, Chemisorbed and Dissociated O_2 on Pt(111) Studied by Different Core Level Spectroscopy Methods. *Surf. Sci.* **1995**, *342*, 119–133.
23. Zhao, F.; Ikushima, Y.; Shirai, M.; Ebina, T.; Arai, M. Influence of Electronic State and Dispersion of Platinum Particles on the Conversion and Selectivity of Hydrogenation of an α,β-Unsaturated Aldehyde in Supercritical Carbon Dioxide. *J. Mol. Catal., A* **2002**, *180*, 259–265.
24. Aricò, A. S.; Shukla, A. K.; Kim, H.; Park, S.; Min, M.; Antonucci, V. An XPS Study on Oxidation States of Pt and Its Alloys with Co and Cr and Its Relevance to Electroreduction of Oxygen. *Appl. Surf. Sci.* **2001**, *172*, 33–40.
25. Abe, Y.; Kawamura, M.; Sasaki, K. Preparation of PtO and α-PtO_2 Thin Films by Reactive Sputtering and Their Electrical Properties. *Jpn. J. Appl. Phys., Part 1* **1999**, *38*, 2092–2096.
26. Sivalingam, G.; Nagaveni, K.; Hegde, M. S.; Madras, G. Photocatalytic Degradation of Various Dyes by Combustion Synthesized Nano Anatase TiO_2. *Appl. Catal., B* **2003**, *45*, 23–38.
27. Seriani, N.; Mittendorfer, F. Platinum-Group and Noble Metals under Oxidizing Conditions. *J. Phys.: Condens. Matter* **2008**, *20*, 184023.
28. Kästle, G.; Boyen, H.-G.; Weigl, F.; Lengl, G.; Herzog, T.; Ziemann, P.; Riethmüller, S.; Mayer, O.; Hartmann, C.; Spatz, J. P.; *et al.* Micellar Nanoreactors—Preparation and Characterization of Hexagonally Ordered Arrays of Metallic Nanodots. *Adv. Funct. Mater.* **2003**, *13*, 853–861.
29. Spatz, J. P.; Mößmer, S.; Möller, M. Mineralization of Gold Nanoparticles in a Block Copolymer Microemulsion. *Chem.—Eur. J.* **1996**, *2*, 1552–1555.
30. Wertheim, G.; DiCenzo, S. Cluster Growth and Core-Electron Binding Energies in Supported Metal Clusters. *Phys. Rev. B* **1988**, *37*, 844–847.
31. Porsgaard, S. Model Catalysts Studied by Photoemission Spectroscopy at Elevated Pressures, Ph.D. Thesis, Aarhus University, 2012.
32. Powell, C. J.; Jablonski, A. NIST Inelastic Mean Free Path Database, version 1.2, **2010**.
33. Tanuma, S.; Powell, C. J.; Penn, D. R. Calculation of Electron Inelastic Mean Free Paths (IMFPs) VII. Reliability of the TPP-2M IMFP Predictive Equation. *Surf. Interface Anal.* **2003**, *35*, 268–275.
34. Wang, C.-B.; Yeh, C.-T. Effects of Particle Size on the Progressive Oxidation of Nanometer Platinum by Dioxygen. *J. Catal.* **1998**, *178*, 450–456.
35. Chaston, J. C. Reactions of Oxygen with the Platinum Metals. *Platinum Met. Rev.* **1965**, *9*, 51–56.
36. Seriani, N.; Pompe, W.; Ciacchi, L. C. Catalytic Oxidation Activity of Pt_3O_4 Surfaces and Thin Films. *J. Phys. Chem. B* **2006**, *110*, 14860–14869.
37. Zhu, Z.; Tao, F. F.; Zheng, F.; Chang, R.; Li, Y.; Heinke, L.; Liu, Z.; Salmeron, M.; Somorjai, G. A. Formation of Nanometer-Sized Surface Platinum Oxide Clusters on a Stepped Pt-(557) Single Crystal Surface Induced by Oxygen: A High-Pressure STM and Ambient-Pressure XPS Study. *Nano Lett.* **2012**, *12*, 1491–1497.
38. Alcock, C. B.; Hooper, G. W. Thermodynamics of the Gaseous Oxides of the Platinum-Group Metals. *Proc. R. Soc. London, Ser. A* **1960**, *254*, 551–561.
39. Rubel, M.; Pszonicka, M.; Ebel, M. F.; Jablonski, A.; Palczewska, W. Oxygen Generated Platinum, Rhodium and Palladium Volatile Losses from Pure Metals and Their Alloys. *J. Less Common Met.* **1986**, *125*, 7–24.
40. Lamber, R.; Romanowski, W. Dispersion Changes of Platinum Supported on Silica Glass during Thermal Treatment in Oxygen and Hydrogen Atmospheres. *J. Catal.* **1987**, *105*, 213–226.
41. Romanowski, W.; Lamber, R. Dispersion Changes and Reactivity of Platinum on Silica during Thermal Treatment under Vacuum and at Low Oxygen Pressure. *Thin Solid Films* **1985**, *127*, 139–158.
42. Harris, F. Growth and Structure of Supported Metal Catalyst Particles. *Int. Mater. Rev.* **1995**, *40*, 97–115.
43. Chu, Y. F.; Ruckenstein, E. On the Sintering of Platinum on Alumina Model Catalyst. *J. Catal.* **1978**, *55*, 281–298.
44. Ogletree, D. F.; Bluhm, H.; Lebedev, G.; Fadley, C. S.; Hussain, Z.; Salmeron, M. A Differentially Pumped Electrostatic Lens System for Photoemission Studies in the Millibar Range. *Rev. Sci. Instrum.* **2002**, *73*, 3872.
45. Grass, M. E.; Karlsson, P. G.; Aksoy, F.; Lundqvist, M.; Wannberg, B.; Mun, B. S.; Hussain, Z.; Liu, Z. New Ambient Pressure Photoemission Endstation at Advanced Light Source Beamline 9.3.2. *Rev. Sci. Instrum.* **2010**, *81*, 053106.
46. Shirley, D. A. High-Resolution X-ray Photoemission Spectrum of the Valence Bands of Gold. *Phys. Rev. B* **1972**, *5*, 4709–4714.